Optics Letters

Rewritable photonic integrated circuits using dielectric-assisted phase-change material waveguides

Forrest Miller,[1,2] Rui Chen,[1] Johannes E. Fröch,[1,3] Hannah Rarick,[3] Sarah Geiger,[4] and Arka Majumdar[1,3,*]

[1]*Department of Electrical and Computer Engineering, University of Washington, 185 E Stevens Way NE, Seattle, Washington, USA*
[2]*Draper Scholar, The Charles Stark Draper Laboratory, 555 Technology Square, Cambridge, Massachusetts, USA*
[3]*Department of Physics, University of Washington, 3910 15th Ave. NE, Seattle, Washington, USA*
[4]*The Charles Stark Draper Laboratory, 555 Technology Square, Cambridge, Massachusetts, USA*
*arka@uw.edu

Photonic integrated circuits (PICs) can drastically expand the capabilities of quantum and classical optical information science and engineering. PICs are commonly fabricated using selective material etching, a subtractive process. Thus, the chip's functionality cannot be substantially altered once fabricated. Here, we propose to exploit wide-bandgap non-volatile phase-change materials (PCMs) to create rewritable PICs. A PCM-based PIC can be written using a nanosecond pulsed laser without removing any material, akin to rewritable compact disks. The whole circuit can then be erased by heating, and a new circuit can be rewritten. We designed a dielectric-assisted PCM waveguide consisting of a thick dielectric layer on top of a thin layer of wide-bandgap PCMs Sb_2S_3 and Sb_2Se_3. The low-loss PCMs and our designed waveguides lead to negligible optical loss. Furthermore, we analyzed the spatiotemporal laser pulse shape to write the PICs. Our proposed platform will enable low-cost manufacturing and have a far-reaching impact on the rapid prototyping of PICs, validation of new designs, and photonic education. © 2023 Optica Publishing Group

Introduction. Photonic integrated circuits (PICs) are becoming essential for various applications, including optical communication [1], sensing [2], and quantum information science [3]. While PICs can significantly expand and enhance the performance of these systems, the fabrication methodology for the PICs is complex and expensive: they require high-resolution lithography and etch processes, which must take place in a sophisticated nanofabrication facility [4]. Additionally, these processes are inherently subtractive, i.e., once fabricated, the wafer cannot be used to fabricate other structures. A low-cost method to fabricate PICs and the ability to rewrite the PIC in the same wafer can help with rapid prototyping.

Chalcogenide-based non-volatile phase-change materials (PCMs) provide a promising route to creating such rewritable PICs [5–7]. These PCMs exhibit large changes in their refractive index ($\Delta n > 0.5$) when they undergo structural phase transition between the amorphous (aPCM) and crystalline (cPCM) states [8]. Crystallization can be actuated by holding the PCM above its glass transition temperature (T_g) but below the melting temperature (T_{mp}) until a crystal lattice forms. Amorphization is achieved by melting and rapidly quenching the PCM. Notably, this microstructural phase transition is non-volatile, i.e., no external power is required to maintain the state after the material phase is changed [9]. These PCMs have been cycled thousands of times without degradation [10] and can potentially be switched for more than 10^{12} times [11]. Consequently, PCMs are widely used in rewritable compact disks (CDs) to store information. A writing laser fires pulses to heat segments of the PCMs which, through amorphization or crystallization, write or erase the stored information. The information is then read out using a probing CW laser. However, rewritable CDs are fundamentally different from rewritable PICs. In a CD, the probing light is reflected off the surface, but in PICs, it propagates along the surface. Therefore, to build PICs, PCMs must provide enough refractive index contrast to guide light in-plane while avoiding significant optical loss.

While researchers have already experimentally demonstrated laser-written rewritable meta-optics [12,13] in PCM, an expensive femtosecond laser was used, and the light did not propagate in a waveguide over a long path. Another work demonstrated only one-way writing of PICs in PCM [14], which lacks the rewritable functionality. Some PIC structures have been written in $Ge_2Sb_2Te_5$ (GST) using nanosecond lasers [15], but the waveguide loss was not considered.

Here, we present a design of a rewritable PIC based on PCMs. As the probing light is guided in the high-index crystalline PCM, we must ensure near-zero absorptive loss in the PCM. At 1.55 μm, GST is too lossy, with an extinction coefficient of cGST $\kappa_{cGST} \approx 1$ [16]. However, wide-bandgap PCMs, such as Sb_2S_3 and Sb_2Se_3, are suitable thanks to their low absorption [10]. These wide-bandgap PCMs also exhibit a large enough index contrast between their amorphous and crystalline states ($\Delta n_{SbS} = 0.6$ and $\Delta n_{SbSe} = 0.77$ at 1.55 μm) [10] to

confine an optical mode. The loss can be further reduced via a dielectric-assisted PCM structure [Fig. 1(b)]. The propagation loss is estimated at 0.0100 dB/µm (0.0086 dB/µm) using Sb_2S_3 (Sb_2Se_3). We envision that the probing light will be coupled in and out of the chip using pre-fabricated grating couplers, akin to input/output pins in an electronic integrated circuit [Fig. 1(a)]. Finally, we simulate switching dynamics to select the spatiotemporal pulse shape of the writing laser that best achieves a complete and reversible phase transition. Specifically, we show that a nanosecond pulsed laser can actuate the phase transition with a spatially Gaussian and temporally rectangular shape. Our proposed rewritable PIC platform could democratize PIC prototyping thanks to its low cost and reusability. This frugal innovation can help with educating students and rapid prototyping of PICs to validate designs.

Low-loss PCM waveguides. While wide-bandgap PCMs have negligible loss in the amorphous state, a non-negligible loss is still present in the crystalline state. We investigated prior works on PCM-integrated ring resonators and estimate the refractive index at $\lambda = 1.55\,\mu m$ in the crystalline state to be $n_{cSbS} = 3.33 + 0.016i$ [17], and $n_{cSbSe} = 4.23 + 0.0043i$ [18,19]. We obtained these values by simulating the reported experimental structures and adjusting the extinction coefficient of the PCMs until our simulated loss matched the reported experimental results. The loss in the crystalline state is critical since the probing light is confined in crystalline PCM, which has a higher refractive index than the amorphous phase ($n_{aSbS} = 2.76 + 0i$, $n_{aSbSe} = 3.22 + 0i$) but also a higher loss. If the light is perfectly confined in a cSb_2S_3 (cSb_2Se_3) core, then the unit propagation loss at λ becomes

$$-20\log_{10}\left[\exp\left(-\frac{2\pi}{\lambda}\cdot\kappa_{cSbS(cSbSe)}\right)\right],$$

resulting in a unit loss for cSb_2S_3 (cSb_2Se_3) $\approx 0.56(0.15)$ dB/µm. While the loss is overestimated, owing to the perfect confinement assumption, the result suggests the necessity of careful waveguide design to achieve a low propagation loss.

One straightforward way to reduce the optical loss is to reduce the PCM thickness, which decreases the interaction between the optical mode and the cPCM. Additionally, thick PCMs are generally harder to fully switch, with 70 nm the thickest to date [20]. Moreover, thinner PCM layers enable higher switching endurance [5,21]. However, an extremely thin PCM layer does not provide enough index contrast to guide a mode. We mitigate this trade-off by exploiting a dielectric-assisted PCM waveguide architecture [22], where a thick dielectric layer of Si_3N_4 [23] is deposited on a thin PCM layer [Fig. 1(a)]. This layer may experience small changes in refractive index during writing, but we expect that such changes will be negligible [24]. The optical mode is mainly confined in the dielectric layer, owing to the geometry of the PCM layer, mitigating the absorptive loss of cPCMs. Such a waveguide will be written from the chip's "erased" state, where the PCM layer is uniformly crystalline. A PCM waveguide is created by selectively switching the PCM to the amorphous state. We assume that a layer of PCM with a thickness T_{PCM} will be deposited on 2 µm of thermal oxide (SiO_2) film on a silicon wafer. A conformal capping material is needed to prevent material reflow and oxidation during switching [7]. Therefore, we encapsulate the PCM with 20 nm of atomic layer deposited Al_2O_3 and then deposit a Si_3N_4 layer with thickness T_{clad} to create the material stack [Fig. 1(b)].
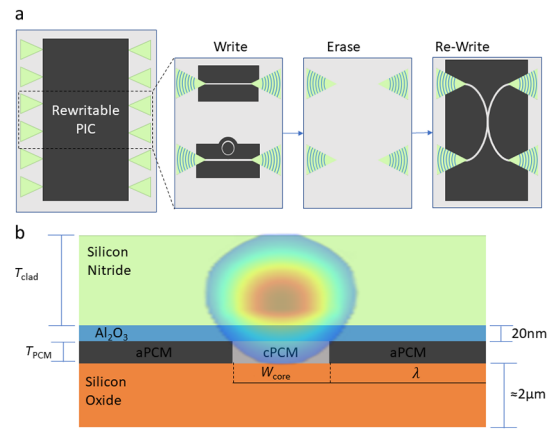

Fig. 1. (a) Proposed rewritable PIC platform. A nanosecond pulsed laser switches the PCM from the crystalline (light gray) to the amorphous (dark gray) phase. The chip can then be uniformly heated to reset the PCM to the crystalline phase, erasing the written PICs. Subsequently, a different PIC can be written in the same region. b) Proposed dielectric-assisted PCM waveguide geometry for low-loss waveguiding. A simulated guided mode is overlaid, depicting a well-confined mode in the dielectric silicon nitride layer for a low propagation loss. Air clads the upper face of the Si_3N_4 layer.
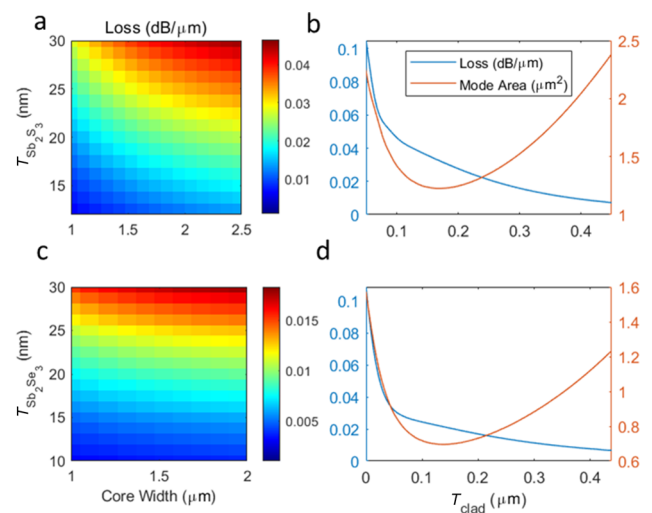

Fig. 2. (a) Waveguide loss (dB/µm) for a joint parameter sweep of the Sb_2S_3 thickness and waveguide core (cSb_2S_3) width. (b) Loss and effective mode area as a function of the Si_3N_4 thickness in the Sb_2S_3 design. (c) Waveguide loss (dB/µm) for a joint parameter sweep of the Sb_2Se_3 thickness and waveguide core (cSb_2Se_3) width. (d) Loss and effective mode area as a function of the Si_3N_4 thickness in the Sb_2Se_3 design.

We optimize the waveguide geometry for low loss, using the finite-element eigenmode solver in Ansys Lumerical (Supplement S1). We start by sweeping the Sb_2S_3 thickness T_{PCM}, and the cSb_2S_3 core width W_{core} [Fig. 2(a)]. Unsurprisingly, a thinner T_{PCM} yields a lower loss. However, below a thickness of 12 nm, the PCM cannot confine a mode. Since the PCM must guide the mode, we find a compromise between loss and mode confinement at a layer thickness of 15 nm and a core width of 2.0 µm. The thickness of the Si_3N_4 layer is designed around 0.4 µm, as

shown in Fig. 2(b). Our optimized structure exhibits a loss of 0.0100 dB/µm.

The loss in the Sb_2Se_3 waveguide exhibits much weaker dependence on W_{core} [Fig. 2(c)]. This is due to the higher real refractive index of Sb_2Se_3, which gives tighter mode confinement. We choose 1.5 µm as the core width to improve integration density. Like the Sb_2S_3 design, the loss increases with increasing T_{PCM}. Here we choose 20 nm as the layer thickness. This T_{PCM} is thin enough to switch and provide low loss while reliably guiding a mode. The Si_3N_4 thickness was set to 400 nm to minimize loss while still confining the mode [Fig. 2(d)]. This geometry demonstrates a loss of 0.0086 dB/µm at 1.55 µm.

We note that while a PCM thickness of 15 nm is sufficient for a straight waveguide, for a bent waveguide, we need slightly thicker PCM or thinner Si_3N_4. Based on our simulation, we found that a T_{PCM} of 25 nm PCM and a 100 nm T_{clad} will be able to guide light across a 75 µm (25 µm) bend using Sb_2S_3 (Sb_2Se_3). These new parameters increase the loss by a factor of eight (four), but support bending, which is critical for any integrated photonic device. With this architecture, we believe that we can optically write directional couplers, Y-splitters, and ring or disk resonators [25]. Components like mode converters or waveguide crossings rely on small features, and our rewritable PIC might not be suitable to write such small features.

Fixed in/out ports using grating couplers. The PICs presented here must interface with free-space optics. We propose to accomplish this using fixed grating couplers on the chip, forming optical input/output ports, between which designs can be written, erased, and rewritten [Fig. 1(a)]. Edge coupling would also work with this design, but we envision grating couplers, enabling easier interfacing. These grating couplers are formed by etching the Si_3N_4 layer, since the optical modes for both designs are primarily confined in the Si_3N_4 layer [Fig. 1(b)]. While this etching step is exactly what we intend to eliminate, we note that, after this one etch, thousands of PIC designs can be written and tested on this platform without further etching. It is possible to write grating couplers into the PCM, but such couplers suffer from low coupling efficiencies and must be rewritten after each anneal. We optimize these gratings for maximum coupling efficiency using single-mode fibers at 25° of incidence using Lumerical's finite-difference time domain (FDTD) simulation (Supplement S2). In the Sb_2S_3 design, a grating pitch of 1.01 µm, a duty cycle of 0.8, and an etch depth of 180 nm resulted in a coupling efficiency of 21%. In the Sb_2Se_3 design, a grating pitch of 0.97 µm, a duty cycle of 0.56, and an etch depth of 240 nm also resulted in a coupling efficiency of 21%. The gratings are connected to the waveguides via a tapered section with end width of 4 µm for both PCMs, which yields a mode overlap of more than 95% with the guided modes.

Spatiotemporal pulse shaping. The PICs can be arbitrarily patterned using a pulsed laser and a three-axis translation stage. We simulated four pulse schemes with different spatiotemporal pulse shapes [Figs. 3(a) to 3(d)] in COMSOL Multiphysics and selected the pulse that best amorphizes the PCM. We expect the ideal shape to be a rectangular spatial shape to provide a smooth boundary region and an increasing temporal shape to produce uniform switching in the depth direction. However, we found that a Gaussian spatial shape and rectangular temporal shape can switch thin Sb_2S_3, offering a simple experimental realization. Pulses of 450 nm wavelength were delivered directly to the 15 nm film of cSb_2S_3 ($n = 4.12 + 1.80i$) in Fig. 1(b), so reflection off the alumina and Si_3N_4 layers was not considered. The pulses
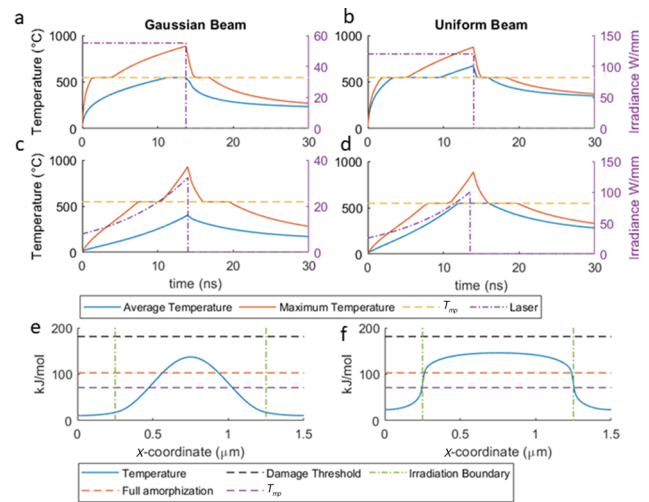

Fig. 3. (a)–(d) Transient thermal dynamics for different pulses: (a) temporally rectangular, spatially Gaussian; (b) temporally rectangular, spatially uniform; (c) temporally exponentially decaying, spatially Gaussian; (d) temporally exponentially decaying, spatially uniform. (e), (f) Static temperature profile along the spatiotemporal line cut at $y = T_{SbS/2}$ and $t = 14$ ns for (e) spatially Gaussian beam and (f) spatially uniform beam. The Gaussian beam switches a smaller area of Sb_2S_3 than the uniform beam, but the uniform beam has a shorter boundary region (the distance between T_{mp} and full amorphization). Thus a Gaussian beam can write finer features, but a uniform beam will probably have better mode confinement.

had either a Gaussian or uniform spatial distribution and either a rectangular or exponentially decaying temporal distribution. All pulses lasted approximately 14 ns and the power was adjusted to achieve a maximum temperature of approximately 900°C.

A successful amorphization pulse must satisfy four conditions. First, enough thermal energy must be applied to melt the PCM completely. This requires the delivered energy to heat PCM to its melting temperature and further overcome the latent heat, given by the multiplication of enthalpy of fusion (H_f) and mass of the PCM. Second, the cooling rate must exceed ~1 K/ns [8]. This ensures that the PCM is frozen in the amorphous state [26] and does not undergo unintentional recrystallization. Third, the absorbed thermal energy must not heat the PCM above its boiling point T_b, which irreversibly ablates the material. We obtain Sb_2S_3 parameters from the literature for the simulations: the melting point is $T_{mp} = 547°C$ [10], the enthalpy of fusion is $H_f = 47.9$ kJ/mol, the boiling point is $T_b = 1149°C$, the density is 4.56 g/cm³ [27], the specific heat is 575.4 J/(kg*K), and the thermal conductivity is 0.42 W/(m*K) [17]. Material parameters for Si_3N_4, Al_2O_3, and SiO_2 are found from COMSOL's materials library (Supplement S3). Lastly, the boundary region between switched and non-switched regions defines the waveguide edge. This boundary contains material heated to its melting point but not enough to exceed its enthalpy of fusion. This implies a partial amorphization, where a portion of the crystalline structure remains. This is undesirable, as a more abrupt index change at the boundary could lead to better mode confinement.

We examine different pulse conditions against these criteria. As shown in Figs. 3(a) to 3(d), all pulse conditions exceed the melting point and achieve a faster cooling rate than 1 K/ns. Our hypothesis with temporal modulation was that the exponential ramp would more uniformly heat the PCM layer along its

thickness in the vertical direction. This statement is supported by the more linear average temperature curve in Figs. 3(c) and 3(d). However, since the Sb_2S_3 layer is very thin, there was little variation in temperature from the top to the bottom of the PCM film. Therefore, we can consider pulses with rectangular temporal modulation. In a thicker PCM layer, we expect that temporal modulation of the beam power could enable more uniform heating in the depth direction.

The performance difference between the spatial beam shapes is apparent in the feature size and the boundary region width. A Gaussian mode is better if the desired circuit requires fine features. This is a direct result of the narrower intensity distribution of a Gaussian compared with a uniform beam. With a Gaussian beam, the width of the switched PCM could be smaller than the laser's spot size if the laser power is tuned such that the beam's full width at half maximum is lower than the amorphization threshold. A uniform beam lacks this ability to achieve a small feature size. However, its advantage is a narrower boundary region in the PCM. The boundary region for the Gaussian beams traverses a distance of 105 pm [Fig. 3(e)]. In comparison, the boundary is only 27 pm [Fig. 3(f)] for a spatially uniform beam. This shorter boundary resembles the step-index profiles used in our previous simulations and leads to better mode confinement. Our thermal simulation verifies that the thin PCM layer can be switched entirely with nanosecond laser pulses and offers a simple experimental realization with a natural laser beam with a Gaussian spatial and rectangular temporal shape.

Conclusion. In conclusion, we have proposed and numerically verified a rewritable, cost-efficient PIC platform using wide-bandgap PCMs and a cost-efficient nanosecond pulse laser. PICs are envisioned to be written (amorphized) by nanosecond laser pulses and erased (crystallized) by rapid thermal annealing or even a simple hotplate. We have designed a dielectric-assisted PCM waveguide configuration, allowing low propagation loss for both Sb_2Se_3 and Sb_2S_3. Efficient grating couplers, working as optical I/O ports, were optimized for both types of waveguide. Comprehensive thermal transfer dynamic simulations were used to verify and select a desirable spatiotemporal pulse condition to ensure complete amorphization with nanosecond pulses. This etch-free platform could accelerate PIC fabrication and testing, potentially democratizing PIC fabrication.

Disclosures. The authors declare no conflicts of interest.

Data availability. Data underlying the results presented in this paper are not publicly available at this time but may be obtained from the authors upon request.

Supplemental document. See Supplement 1 for supporting content.

REFERENCES

1. K. Wang, A. Nirmalathas, C. Lim, E. Wong, K. Alameh, H. Li, and E. Skafidas, Opt. Lett. **43**, 3132 (2018).
2. L. He, H. Li, and M. Li, Sci. Adv. **2**, 1 (2016).
3. J. Wang, F. Sciarrino, A. Laing, and M. G. Thompson, Nat. Photonics **14**, 273 (2020).
4. J. A. Liddle, J. Bowser, B. R. Ilic, and V. Luciani, J. Res. Natl. Inst. Stan. **125**, 125009 (2020).
5. R. Chen, Z. Fang, F. Miller, H. Rarick, J. E. Fröch, and A. Majumdar, ACS Photonics **9**, 3181 (2022).
6. Z. Fang, J. Zheng, A. Saxena, J. Whitehead, Y. Chen, and A. Majumdar, in *Conference on Lasers and Electro-Optics* (Optica Publishing Group, 2021).
7. Z. Fang, R. Chen, J. Zheng, and A. Majumdar, IEEE J. Sel. Top. Quantum Electron. **28**, 1 (2022).
8. M. Wuttig, H. Bhaskaran, and T. Taubner, Nat. Photonics **11**, 465 (2017).
9. J. Faneca, I. Zeimpekis, S. T. Ilie, T. D. Bucio, K. Grabska, D. W. Hewak, and F. Y. Gardes, Neuromorph. Comput. Eng. **1**, 014004 (2021).
10. M. Delaney, I. Zeimpekis, D. Lawson, D. W. Hewak, and O. L. Muskens, Adv. Funct. Mater. **30**, 2002447 (2020).
11. S. Kim, G. W. Burr, W. Kim, and S.-W. Nam, MRS Bull. **44**, 710 (2019).
12. N. I. Zheludev and Y. S. Kivshar, Nat. Mater. **11**, 917 (2012).
13. Q. Wang, E. T. F. Rogers, B. Gholipour, C.-M. Wang, G. Yuan, J. Teng, and N. I. Zheludev, Nat. Photonics **10**, 60 (2016).
14. D. Mao, M. Chen, X. Ma, A. Soman, H. Xing, T. Kananen, N. Augenbraun, C. Cheng, M. Doty, and T. Gu, Opt. Mater. Express **10**, 2126 (2020).
15. K. Chaudhary, M. Tamagnone, X. Yin, C. M. Spägele, S. L. Oscurato, J. Li, C. Persch, R. Li, N. A. Rubin, L. A. Jauregui, K. Watanabe, T. Taniguchi, P. Kim, M. Wuttig, J. H. Edgar, A. Ambrosio, and F. Capasso, Nat. Commun. **10**, 4487 (2019).
16. J. Zheng, A. Khanolkar, P. Xu, S. Colburn, S. Deshmukh, J. Myers, J. Frantz, E. Pop, J. Hendrickson, J. Doylend, N. Boechler, and A. Majumdar, Opt. Mater. Express **8**, 1551 (2018).
17. R. Chen, Z. Fang, C. Perez, F. Miller, K. Kumari, A. Saxena, J. Zheng, S. J. Geiger, K. E. Goodson, and A. Majumdar, "Non-volatile electrically programmable integrated photonics with a 5-bit operation," arXiv, arXiv:2301.00468 (2023).
18. C. Ríos, Q. Du, Y. Zhang, C.-C. Popescu, M. Y. Shalaginov, P. Miller, C. Roberts, M. Kang, K. A. Richardson, T. Gu, S. A. Vitale, and J. Hu, PhotoniX **3**, 26 (2022).
19. Z. Fang, R. Chen, J. Zheng, A. I. Khan, K. M. Neilson, S. J. Geiger, D. M. Callahan, M. G. Moebius, A. Saxena, M. E. Chen, C. Rios, J. Hu, E. Pop, and A. Majumdar, Nat. Nanotechnol. **17**, 842 (2022).
20. K. Gao, K. Du, S. Tian, H. Wang, L. Zhang, Y. Guo, B. Luo, W. Zhang, and T. Mei, Adv. Funct. Mater. **31**, 2103327 (2021).
21. R. Chen, Z. Fang, J. E. Fröch, P. Xu, J. Zheng, and A. Majumdar, ACS Photonics **9**, 2142 (2022).
22. F. Qiu, H. Sato, A. M. Spring, D. Maeda, M.-a. Ozawa, K. Odoi, I. Aoki, A. Otomo, and S. Yokoyama, Appl. Phys. Lett. **107**, 123302 (2015).
23. J. Kischkat, S. Peters, B. Gruska, M. Semtsiv, M. Chashnikova, M. Klinkmüller, O. Fedosenko, S. Machulik, A. Aleksandrova, G. Monastyrskyi, Y. Flores, and W. T. Masselink, Appl. Opt. **51**, 6789 (2012).
24. G. D. Paoli, S. L. Jantzen, T. D. Bucio, I. Skandalos, C. Holmes, P. G. R. Smith, M. M. Milosevic, and F. Y. Gardes, Photonics Res. **8**, 677 (2020).
25. F. Qiu, A. M. Spring, H. Miura, D. Maeda, M.-a. Ozawa, K. Odoi, and S. Yokoyama, ACS Photonics **3**, 780 (2016).
26. M. Wuttig and N. Yamada, Nat. Mater. **6**, 824 (2007).
27. J. R. Rumble, *CRC Handbook of Chemistry and Physics*, 97th ed. (2022).